



Influence of volume loss for the fragment replacement method (FRM) in three dimensions

Shuang Jiao¹, Chengshun Xu^{1,*} , Jialin Xu¹, and Chenglong Jiang¹

¹The Key Laboratory of Urban Security and Disaster Engineering of Ministry of Education, Beijing University of Technology, Beijing 100124, China

Received: 25 November 2022

Accepted: 27 January 2023

Published online:

7 February 2023

© The Author(s), under exclusive licence to Springer Science+Business Media, LLC, part of Springer Nature 2023

ABSTRACT

The impact of crushing on the macroscopic mechanical characteristics of granular materials from a microscopic perspective has recently been revealed using the discrete element method (DEM). The influence of the self-organized, mass conservation and volume conservation of daughter particles in the fragment replacement method (FRM) on particle breakage is complex and crucial. In this paper, 14-ball Apollo directly filling method (DFM) and expansion method are combined to keep balance among particles before and after crushing, considered to establish DEM to simulate granular material. By considering the influence of volume loss on the micro-fracture condition of the samples, the macro-responses of mechanical and deformation characteristics, the gradation change and the critical state are studied. The effect of inter-particle interaction on macroscopic properties is also analyzed from the microscopic perspective. The rationality of the volume expansion method is verified. The comparisons of samples with volume conservation and volume loss show that the stress development process and the volumetric strain are affected. The existence of the balance point of volume effect is related to the stress level which lead to the difference in stress and strain. Through analysis of relative breakage index (B_r) and the statistical number of microscopic particles, it can be seen that the gradation deviation comes from the two-way influence of the volume loss on the crushing of particles. The volume loss has no effect on stress ratio in the critical state, but has a significant effect on stress change during shearing process, and results in the critical state void ratio to decrease with increasing confining pressure. The rationality of daughter particles' volume conservation are analyzed from the motion, displacement development and force chain evolution.

Handling Editor: M. Grant Norton.

Address correspondence to E-mail: xcs_2017@163.com

<https://doi.org/10.1007/s10853-023-08260-6>

Introduction

As typical granular materials, geotechnical materials have crushing characteristics. Rockfill, gravel, calcareous sand, and other easily broken particles [1–3] are widely used as main building materials in dam construction, foundation filling of high-speed railways, and offshore engineering, which are related to the long-term safety of the project. The crushing of granular materials will significantly affect the overall strength and deformation characteristics of the soil. Therefore, it is of great significance for related engineering research to explain the crushing laws and their macro- and micro-characteristics responses.

At present, the traditional method of obtaining the stress–strain and shear band changes of samples through experiments and the Discrete Element Method (DEM), which was originally described by Cundall et al. [4] in the 1970s, are applied to the study of particle crushing. Coop et al. [5] conducted a series of ring shear tests to study the variation of calcareous sand breaking with strain. Ghafghazi [6] and Yu [7] investigated characteristics of particle breakage with different stress levels in triaxial shear. Although the results of the experimental method are more intuitive, the method has the disadvantage that the specimens and experimental conditions cannot be accurately replicated, which will inevitably lead to unnecessary errors. The DEM allows precise control of external stress conditions while satisfying the reproducibility of samples. It is well suited to understand the motion between a given combination of particles during loading and is applied to develop and verify the intrinsic relationships of soils, providing an important avenue for particle fragmentation studies. There are mainly two DEM methods to simulate particle breakage: one is the Bonded-Particle Method (BPM) [8], in which multiple small particles are bound into one large particle through contact connections. The large particle will be broken, when the force is greater than the set binding force. Cheng et al. [9] applied BPM to simulate single-particle crushing as well as triaxial tests on cubical samples made of 389 agglomerates, which provided valuable insights into plasticity on crushable soils from micromechanics. McDowell and Harireche [10, 11] et al. simulated the fracture of granular materials by this method and further investigated the yield stress of sand based on oedometer tests. BPM is suitable for

simulating particles of different shapes and can reflect the strength characteristics of particle breakage and complex interactions between particles to a certain extent. However, the strength and size effects can only be well reflected if the premise of large-scale particle aggregate crushing is satisfied, which leads to a significant reduction in computational efficiency. And most critically, the internal sub-particles cannot be crushed multiple times. Another method is the Fragment Replacement Method (FRM), which replaces the parent particle with a series of inner-filled daughter particles when fragmentation occurs. Lobo-Guerrero and Vallejo [12] obtained the sub-particle evolution law by simulating two-dimensional particle fragmentation, but the discussion of critical void fraction under two-dimensional conditions is very limited. Marketos and Bolton [13] investigated the particle cementation bond strength and fragmentation condition for the compacted region by three-dimensional DEM, which provided an idea for the study of compaction band initiation and propagation. FRM has the advantage of high computational efficiency, but the accuracy of the simulation results depends on the determination of particle failure criterion and arrangement of the daughter particles. De Bono and McDowell [14, 15] performed a series of one-dimensional normal compression simulations of granular materials but did not address the mass loss problem in crushing. The two main problems of the FRM are the mass conservation (volume conservation) and the number of the generated daughter fragments, which have been studied by many scholars on these two points [16–18]. Bun-Nun et al. [19] used a self-organized form of split particles without mutual overlap, which can avoid additional inter-particle forces, but the discriminant condition for fragmentation is still the characteristic strength of individual particles and does not fully consider the effect of local stress concentration in the particles. To ensure mass conservation, Shi et al. [20] used BPM for the first crushing and FRM method for subsequent crushing. But this method still has a non-negligible mass loss for the re-crushing of particles with larger particle size. Cleary [21] and Sinnott [22] improved the organization pattern of sub-particles to reduce the mass loss to some extent, but their results were not the actual grade change. Li [23] et al. used overlapped particles to substitute, which ensured the conservation of mass and volume and reflected the real gradation change. But additional work is introduced in

the process of breakage, which changes the condition of contact force and results in the change of crushing amount. While most of the existing studies on the conservation of mass focus on the fragmentation evolution law after the improved self-organization pattern, and rarely study the effect of volume loss on macroscopic properties under the change of confining pressure. However, the effect of volume differences on the macroscopic mechanical properties and the accuracy of simulation results is unclear. Therefore, it is necessary to study the volume conservation problem.

Breakage is defined as the process of turning large particles into small ones under the action of external forces. The problem of volume conservation mainly arises from the form of self-organization of daughter particles during the fragmentation of parent particles to secondary particles. The contact rupture between BPM clusters can visually reflect the particle crushing state, but the accuracy of the results is limited by the particle base. While the breakage of FRM reflects the real crushing situation. The triaxial compression process of fracturable materials is accomplished by both particle rearrangement and particle breakage. Cracking occurs when the local force state of the particles exceeds a given threshold during compaction, and the crack extends from the contact point leading to crushing. The existing failure criteria can be divided into two categories, respectively, the overall particle stress state and the maximum contact force acting on the particle as a criterion to discriminate crushing. The overall stress of the particles is mostly based on the classical fracture criterion, and the average particle stress is usually considered. Such as McDowell et al. [15, 24, 25] applying the Von Mises criterion, Zhou et al. [26] applying the Mohr–Coulomb criterion, and Ben-Nun et al. [27] applying the Drucker-Prager criterion are from this perspective. However, it is also therefore necessary to introduce additional factors to consider the stress concentration in the formulation. When the overall stress does not meet the crushing conditions, the local stress exceeding the ultimate strength of the particle may still cause crushing. Because of the phenomenon of stress concentration, using the maximum contact force of the particles as the limit condition for judging crushing [20] is more in line with the actual crushing situation. Jaeger [28] suggested that the tensile strength of an individual particle can be defined as its failure tensile stress. Therefore, it is more reasonable

to use the maximum contact force as the criterion for breakage.

To sum up, this paper combines the discrete element method with different FRM daughter particle self-organization modes to consider the effect of newly spawned particles' volume loss introduced by breakage. By establishing a discrete element triaxial compression model, the role of the volume effect in the variation of specimen grain size distributions (GSDs), the stress–strain characteristics, and the critical state is further discussed. The effect of the particle motion law on the macroscopic properties is analyzed from the microscopic point of view, and then the rationality of using the expansion method to maintain volume conservation is verified.

DEM model of particle breakage

Particle failure criteria

The particle failure criteria need to relate the limitation on certain characteristic strengths to the contact forces acting on the particles. In this paper, the stress concentration in the particle contact process is considered, and the simulation is carried out using the maximum contact force. Fracturing and compression simulations performed by De Bono and McDowell [14, 15, 29] for silica sand used two different particle failure criteria and investigated in detail their correctness under normal compression conditions. Russell et al. [30] obtained a two-parameter maximum contact force breakage criterion by performing point load tests on a single spherical particle, which provided a more reliable estimate of compressive strength, and extended it to compression tests with different particle sizes. He [31] then proved that the criterion is also applicable to spherical particle groups with different coordination numbers and indicates that rupture occurs when the maximum contact force exceeds a threshold particle strength value. Under the assumption that the sphere is elastic, κ_{mob} at any point will be proportional to the applied load. As the applied load is increased, the maximum κ_{mob} attains a value equal to the available strength κ . Therefore, the relationship between the limit condition can be expressed as

$$\kappa_{\text{mob}} \leq \kappa \quad (1)$$

where κ_{mob} is the mobilized strength and κ is the intrinsic strength, which is related to the uniaxial tensile and compressive strengths.

When a sphere is subjected to contact forces, a certain amount of this available strength, denoted by mobilized strength κ_{mob} , will use up. The forces are assumed to act normal with a small area on the surface of the sphere defined by the subtended angle θ_0 and radius R (Fig. 1). The symmetrical maxima of κ_{mob} is located on and near the diameter of the connecting load center. Under the above stress conditions, the value of mobilized strength κ_{mob} can be expressed as Eq. (2). When θ_0 is small, ρ given by Hiratsu and Oka [32] can be approximately regarded as the average pressure obtained by dividing the contact force F by the action area A_f .

$$\kappa_{mob} = f(\chi, \nu) \frac{F}{\pi R^2 \sin^2 \theta_0} \tag{2}$$

$$f(\chi, \nu) = \frac{\sqrt{3}(1 + \chi^2) \cdot \left[\frac{3}{32} + \frac{\sqrt{2}}{24} \left(\frac{\sqrt{2}}{12} - \frac{1}{4} \right) \nu + \left(\frac{1}{2} - \frac{\sqrt{2}}{3} \right) \right] \nu^2}{\chi (2 - \sqrt{2})(1 + \nu)} \tag{3}$$

$$A_f = \pi R^2 \sin^2 \theta_0 \tag{4}$$

$$\rho = \frac{F}{A_f} \tag{5}$$

where ν is the Poisson ratio; χ is a parameter that reflects the microstructural properties of the material, $f(\chi, \nu)$ is shown in Eq. (3) as a function of the Poisson

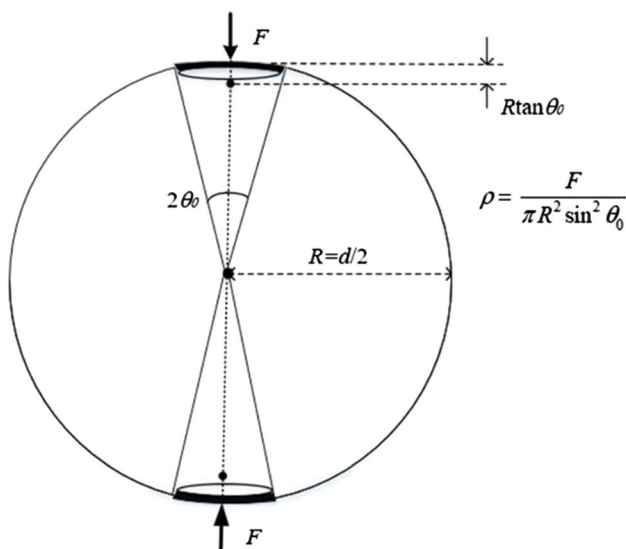


Figure 1 Range of spherical particles affected by point load and induced equivalent stress.

ratio of the material and its own properties[30], and its value is between 10 and 170, proposed by Christensen [33]; F is the load value of the particle; R is the radius of sphere; θ_0 is the central angle enclosed by the edge point radius and the normal radius through the action of the normal force F . In general, the stresses acting on a given particle can be defined as a second-order tensor in discrete element method. The stress tensor can be expressed as

$$\sigma_{ij} = \frac{1}{V} \sum_{N_c} I_i^c J_j^c \tag{6}$$

where V is the volume of the particle, N_c is total number of contacts on the particle, I_i^c is the i -th component of contact vector, and J_j is the force acting on j -th component of the contact point. The critical contact force can be obtained from the limit condition

$$F' \geq \frac{\kappa}{f(\chi, \nu)} A_f \Rightarrow \sigma_{lim} = \frac{\kappa}{f(\chi, \nu)} \tag{7}$$

From Eq. (7), it can be seen that the ultimate force F' is affected by the ultimate strength σ_{lim} of the particle and the contact area of the force A_f . σ_{lim} is related to the experimental material and its value increases with decreasing particle size. As the ultimate strength of single particle follows Weibull statistics distribution [34, 35], the relationship between the σ_{lim} and the tensile strength of the particle σ_n under diametrical loading can be related to size by:

$$\sigma = \sigma_0 \left(\frac{d}{d_0} \right)^{-3/m} \tag{8}$$

$$\sigma_{lim} = 0.9 \sigma_n \tag{9}$$

where σ_0 is the characteristic particle strength at diameter d_0 , which is a value of the distribution such that 37% of the particles survive, m is the Weibull modulus, which decreases with increasing strength.

Self-organization form of fragments

The fragment spawning procedure is another important issue related to particle fragmentation DEM modelling in addition to the particle breakage criterion. The spawned particles are assembled according to the Apollonian sphere packings proposed by Borkovec et al. [36] after a fragmentation event. The limiting fractal dimension of the apollonian packings in most geotechnical materials is close

to that found by Coop et al. [5] for particle fragmentation, with a final value of 2.47. Ciantia et al. [17, 37] studied the number of filled daughter particles in a 3D model and showed that 14 non-overlapping spheres satisfy the accuracy condition while ensuring computational efficiency. But the 14 inscribed daughter spheres of the mother particle, which is called the direct filling method (DFM) here, lost more than 40% of the original particle volume after the first crushing. This results in a mass loss of up to 47% at constant sphere density. To ensure the two conservation principles, the method of linear expansion of the volume of the daughter fragments to satisfy the mass conservation after the original crushing and filling are adopted. An overlap-free spawned particles layout by the expansion method is achieved (Fig. 2), the algorithm is shown in Table 1.

In case of particle fragmentation, the radius and position of the sub-particles can be determined based on Apollo filling. The sub-particles expand as individuals until volume conservation before and after fragmentation is satisfied. In the expansion phase, to avoid local breakage effects caused by excessive sub-particle velocity, a zeroing setting is performed when the velocity exceeds the limit, and multiple expansions are also used to reduce local disturbances.

Crushing causes a local imbalance in the contact of the particles. In this case, the combined forces on the daughter particles can rise abruptly and the force chain including the mother particle breaks, resulting in local collapse. To solve the local imbalance and sub-particle diameter expansion problem, a reduced critical time step in a global–local framework is needed to ensure its stable operation. By means of two discrete dynamic time steps–local time step and global time step, the effects of excessive local stresses between particles as well as internal stress variations can be eliminated by multiple low-velocity expansion in local time step. Thus, the conservation of mass, the conservation of volume and the non-overlapping sub-particle layout are realized. Simplified breakage

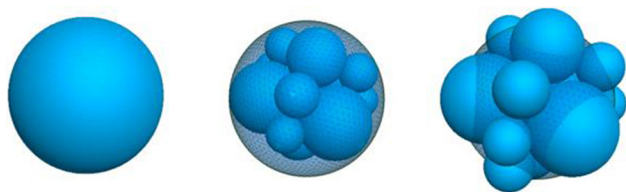


Figure 2 Sub-particle layouts of FRM after breaking with apollo filling.

Table 1 Sub-particle expansion algorithm

Algorithm Sub-particle expansion algorithm
I_e - Iterations for expansion
E_b - Breakage events in one step
P_s - Sub-particle becomes to an individual
V_s - Velocity of sub-particle
Input: Radius and position of the sub-particles
If $E_b = \text{True}$
Initial particle formation
For P_s do
While Iteration $\leq I_e$ do
For each particle in P_s do
If local V_s exceed the limit then
Set spin and velocity to zero
Else
Translate and expand particle
end if
end for
end while
end for
end if
Output: Updated configuration of sub-particles

algorithm is shown in Fig. 3. The particles are discriminated according to the contact force and particle position under the global time step. If no fragmentation occurs, the particle remains under the global time step. If fragmentation occurs, the IDs and positions of sub-particles are updated in the local time step. The sub-particles undergo iterative expansion. In particular, under the expansion process, the values of spin and velocity are set to 0 in order to avoid the extra kinetic energy caused by expansion. After the expansion is completed, the parent particle is replaced by the sub-particle cluster and the parent particle is deleted.

Figure 3 Simplified breakage algorithm.

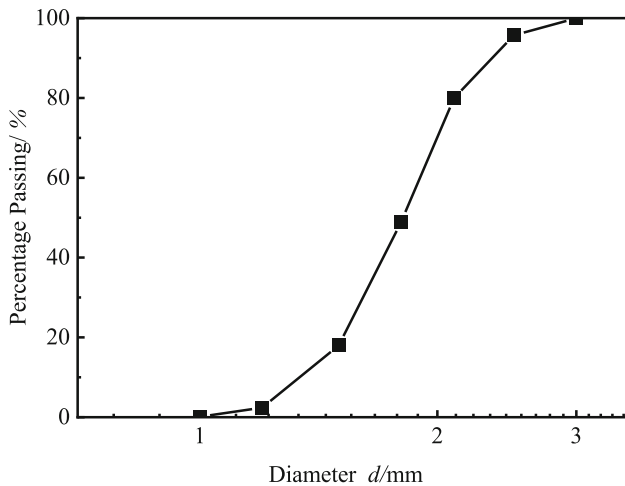
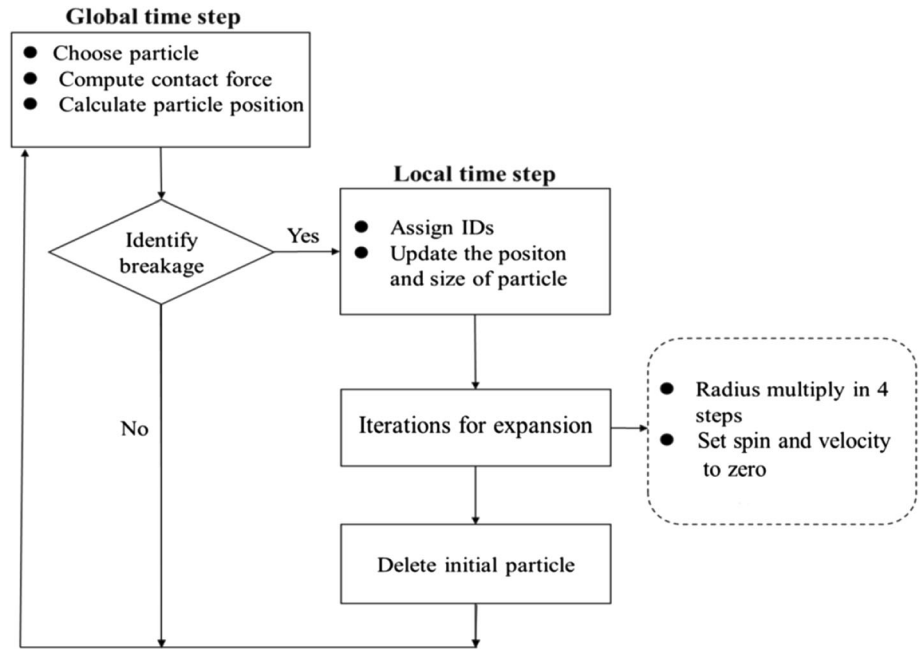


Figure 4 Initial gradation curve of different crush methods.

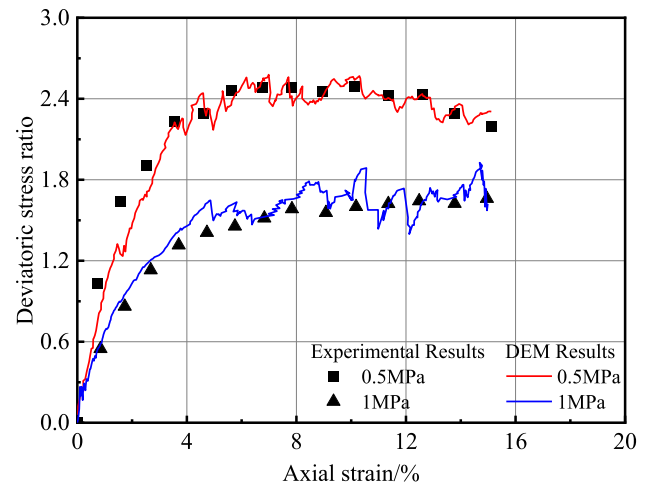


Figure 5 Simulation of triaxial test results of calcareous sand.

Discrete element model validation

A series of numerical triaxial tests were performed to simulate drained shear conditions. In this paper, a cylindrical particle aggregate with a height of 40 mm and a diameter of 20 mm was used as the specimen in the numerical model, and the minimum particle size that could be crushed was set at $d_{lim} = 0.25 d_{min}$, which d_{min} was the minimum particle size of the initial material. Both physical test and numerical simulations use specimens with the same gradation distribution. Physical triaxial tests are irregularly shaped particles, while numerical simulations are

spherical particles. The particle size of the assembly ranges from 1 to 3 mm. The initial specimen particle size is adopted from the test gradation in Fig. 4. Percentage passing is the percentage of the total mass of the specimen by the mass of a particle passing through a certain millimeter mesh sieve. Since the study of the effect of volume loss on the simulation was the main purpose, the stress variation of the numerical method was calibrated mainly using the results of triaxial tests of calcareous sand in Fig. 5 to determine the corresponding particle parameters and particle fragmentation criterion parameters. In the soil mechanics, the compression direction is taken as

Table 2 Input parameters of FRM method for simulation

Input parameter	Value
Contact law	Hertzian
Smallest particle diameter, d_{min} : mm	1.0
Voids ratio	0.63
Density, ρ_s :kg/m ³	2790
Initial number of particles	2929
Shear modulus, G : GPa	0.08
Poisson’s ratio, ν :	0.3
Particle friction coefficient, f_u	0.57
Wall friction coefficient	0.2
Weibull modulus, m	10.0
Limit strength of characteristic particle, $\sigma_{lim,0}$:MPa	500
Comminution limit, d_{lim} :mm	$0.25 d_{min}$

the positive direction. The ratio of $\sigma_1 - \sigma_3$ to σ_3 is the deviatoric stress ratio and the difference between the deformation length and the original length of the specimen axially divided by the original length is the axial strain. It can be seen that the discrete element model is in general agreement with the macroscopic stress–strain characteristics of the physical tests under different confining pressures. In critical state soil mechanics, the state in which shear drives granular soil toward a state of constant volume and constant shear stress at a constant mean stress is called the critical state. [38] In the triaxial compression test, the critical state needs to be reached at a larger axial strain. 30% of the termination strain is selected in the text. The average value in the strain range of 29%–

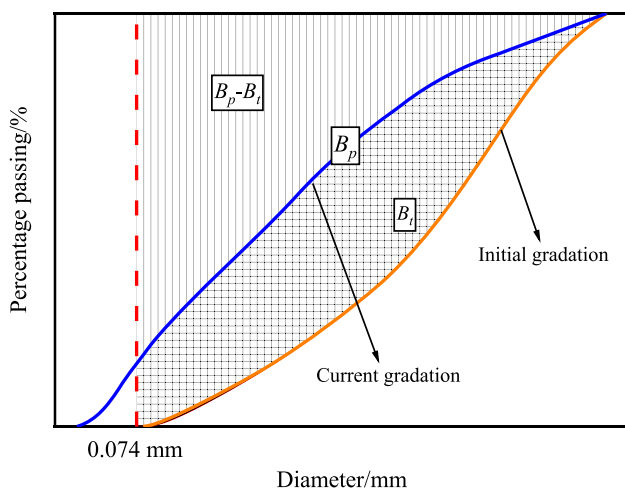


Figure 6 Illustration for relative breakage ratio of particle crushing amount.

30% is chosen as the representative value of the critical state.

To validate the DEM model, the input parameters are shown in Table 2. The Hertzian contact model was used [15, 17]. In the plane of void ratio and spherical stress, the critical state line needs to be determined by sufficient critical state points. Therefore, in this paper, five confining stress levels, i.e., 50 kPa, 100 kPa, 500 kPa, 1 MPa, and 2 MPa are used and 0.63 is used as the initial void ratio. The model tests aim to reveal the effect of volume conservation on the deformation characteristics, macroscopic gradation differences, and critical state of the specimens.

Analysis of numerical test results

To explore the role of volume effects in two forms of daughter particles’ self-organization, a numerical model without particle fragmentation is combined. And the comparison is mainly made in three aspects of grain size distributions, change of stress–strain difference and critical state, and the particle microscopic motion mechanism is analyzed in depth.

Variation of GSDs

Many scholars have proposed different fragmentation parameters by physical experiments to trace the changes in gradation curves [39–42], and the relative breakage ratio (B_r) used in this paper is the concept of relative fragmentation proposed by Hardin to quantitatively describe the GSDs [41], which is shown in

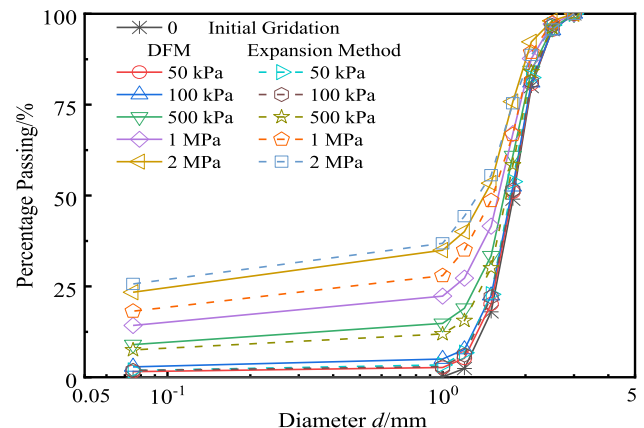


Figure 7 Grain size distributions of two kind of samples under triaxial tests.

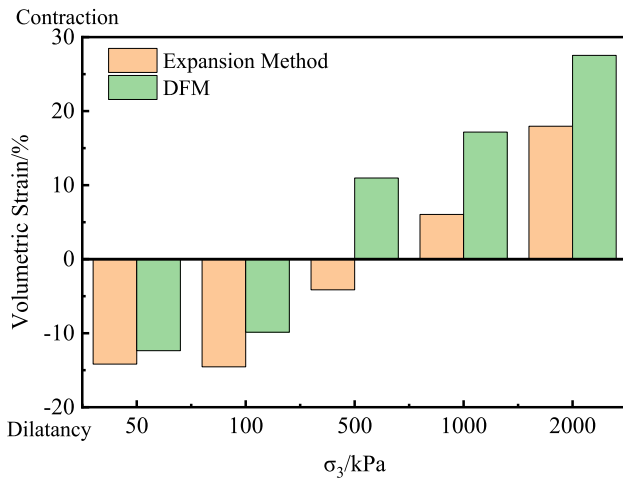


Figure 8 Relationship between volumetric strain and confining pressure after shear completion.

Fig. 6 to describe the gradation distribution quantitatively,

$$B_r = \frac{B_t}{B_p} \tag{10}$$

where B_t is the total breakage potential, defined as the area enclosed by the 0.074 mm size line, the current grading, and the initial grading curve, B_p is the initial breakage potential, which can be expressed as the area surrounded by the initial grading curve and 0.074 mm particle size line.

In the past, the FRM focused more on changes in the number of crushed particles and paid less attention to the post-crushing gradation changes. However, it is worth noting that microscopic volume change has a two-way effect on the macroscale.

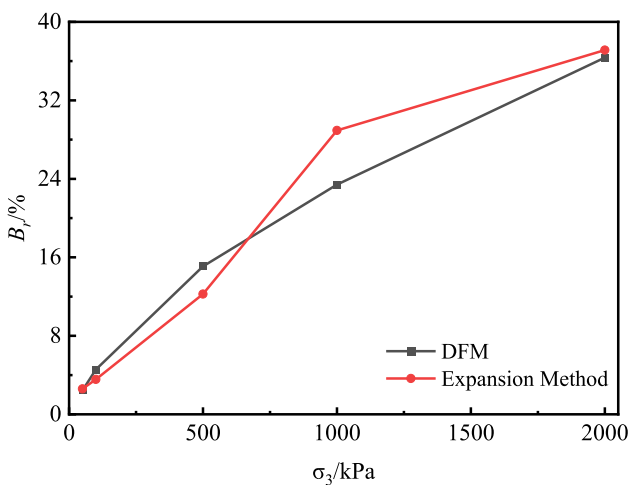


Figure 9 Relationship between B_r and confining pressure.

Table 3 B_r of two samples under different confining pressures

Confining pressure	DFM B_r	Expansion method B_r
50 kPa	0.0244	0.0261
100 kPa	0.0457	0.0356
500 kPa	0.1508	0.1226
1 MPa	0.2341	0.2894
2 MPa	0.3636	0.3713

Figure 7 shows the changes in GSDs in the two methods. At low confining pressure, the crushing amount of both methods is small and has little effect on the gradation. As the confining pressure increases, both gradation curves shift upward, and the difference between the methods is getting bigger, and the expansion method is obviously higher than the directly filling method. Under 2 MPa confining pressure, the difference in grading between the two methods becomes smaller again. Figure 8 shows the volume change after shearing at different confining pressures. It can be seen that the difference in volumetric strain between the two methods is small at low perimeter pressure. The difference between the volumetric strains becomes as the confining pressure increases. At high confining pressures, the difference between volumetric strains becomes smaller again. The reduction of the volume of the filled particles by the Apollo method leads to an upward shift of the grading curve; at the same time, due to the reduction of the sub-particle volume, the ultimate strength of the single-particle increases and further prevents the crushing, which in turn reduces the magnitude of the upward shift of the grading curve. In this paper, while counting the number of crushed and uncrushed particles, the effect of volume loss on the relative breakage ratio is investigated, which in turn quantitatively describes the different patterns reflected by the two filling methods in terms of gradation changes.

The relative breakage ratios caused by the two methods are shown in Fig. 9 and Table 3. B_r of specimens filled directly by the Apollo method under 50 kPa confining pressure is slightly lower than that of the expansion method specimens following volume conservation. By counting the number of particles, it is clear that the volume loss leads to an increase in the ultimate particle strength with little difference in the number of uncrushed particles. At the same time, the crushing volume is less than the

Table 4 Statistics of broken particles and unbroken particles of samples

	50 kPa		100 kPa		500 kPa		1 MPa		2 MPa	
	Broken	Unbroken	Broken	Unbroken	Broken	Unbroken	Broken	Unbroken	Broken	Unbroken
DFM	1519	2827	2451	2675	10868	2199	26834	1891	46827	1473
Expansion Method	1931	2818	5349	2779	18946	2390	43297	1728	70478	1428

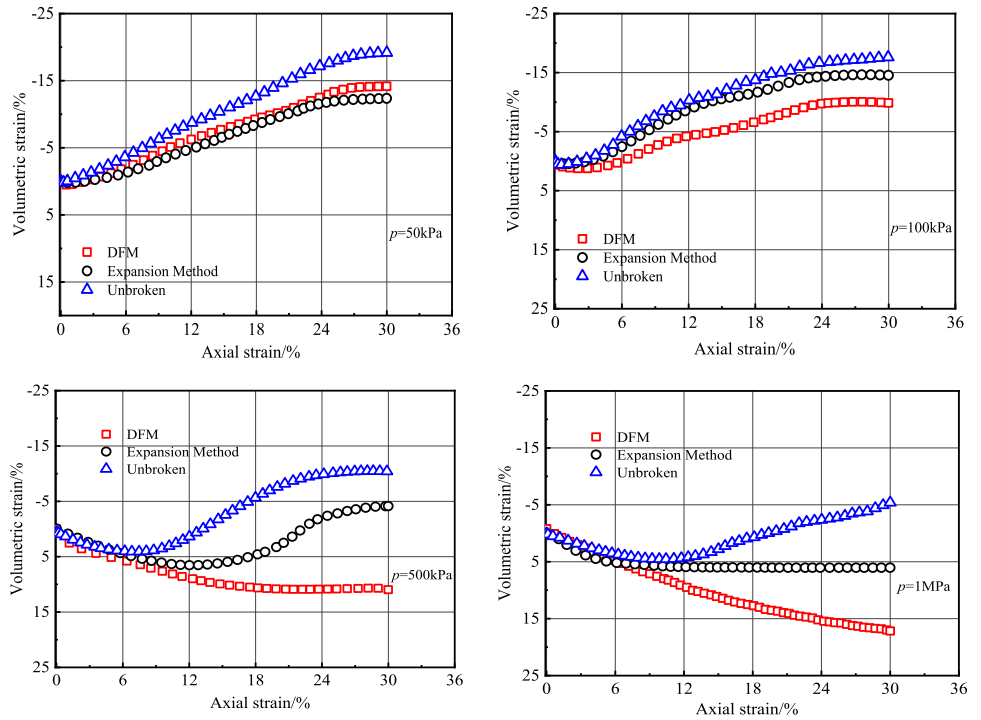
volume conserving specimens obtained by the expansion method due to the limitation of the lower confining pressure level. The differences in the gradation curves at this stage are mainly influenced by the ultimate strength of the sub-particles. However, due to the small amount of crushing, little difference is reflected in the gradation curves. When the confining pressure increases to 100–500 kPa, the difference between the grading curves of different methods is more obvious, and the volume loss of the Apollo method is larger than the volume conservation expansion method. The stress concentration phenomenon caused by the volume reduction of daughter particles due to the change of the confining pressure conditions promotes the fragmentation of adjacent particles in the Apollo method. The particle volume expansion causes the stress concentration effect to be reduced, but the number of broken particles is much higher than that of the directly filling method shown in Table 4, due to the volume effect of the expanded particles reducing the ultimate strength of individual particles, which are the main source of the number of broken particles. The difference in the number of crushed particles at this stage is greater than that at the previous stage. While the number of uncrushed particles for the directly filling method is significantly less than that for the expansion method. Therefore, the main factor causing the upward shift of the grading curve at this stage originates from the number of uncrushed particles. When confining pressure increases to 1–2 MPa, the expansion method specimens upward shift more than the direct Apollo filled specimens. The variability of the grading curves again decreases with the increase of the surrounding pressure. A further increase in stress level leads to more initial particle fragmentation. Larger volume sub-particles have a higher fragmentation probability. With these two effects, the expansion method far exceeds the Apollo direct filling method in terms of the number of crushed particles. Therefore, there exists the equilibrium point of the volume loss effect

mentioned before, which leads to the alternating position of the grading curve. And there is a volume loss point that makes the maximum difference in the gradation curves. Beyond this point, as the confining pressure increases, the two gradation curves start to approach each other and converge to the ultimate crushing curve at the same time.

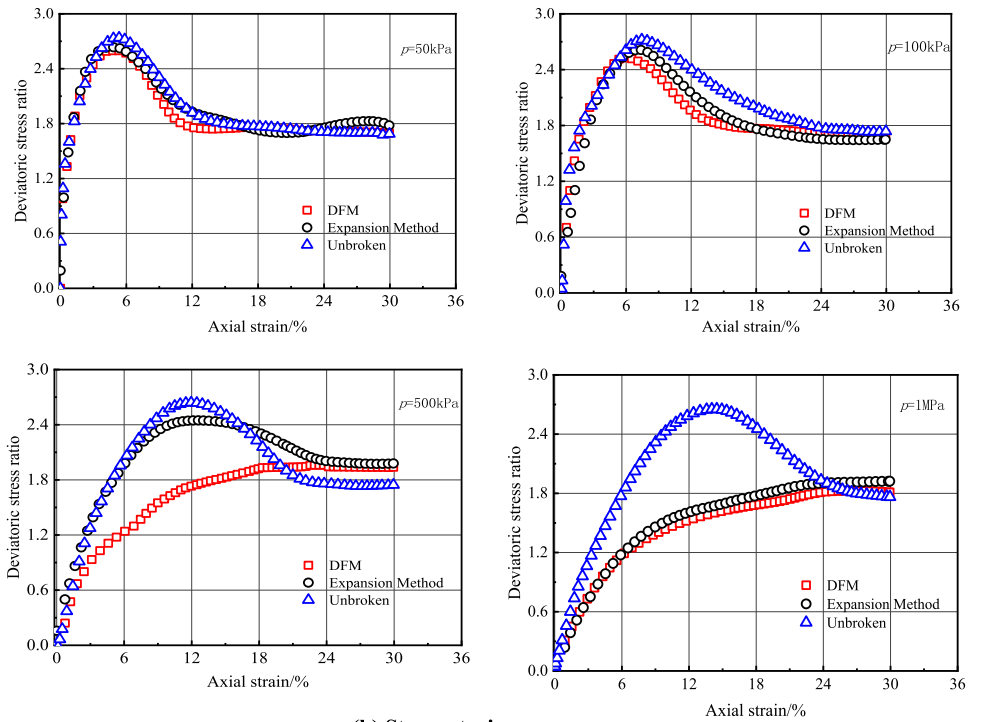
Characteristics of strength and deformation

Previous studies have concluded that the Apollo layout has a small effect on the strength properties of the particles. Figure 10 shows the results of the volumetric strain and stress–strain simulation considering the volume loss factor in this paper. The specimens reached the peak strength at the beginning of shear at a small shear displacement. As the confining pressure increases, the shear strain required to reach the peak strength increases. The post-peak strength undergoes different degrees of stress drop, which is consistent with strain softening characteristics. Under the condition of lower confining pressure, the amount of particle breakage is very small. The unbroken particles play a major role, and the main skeleton of the sample still dominates the stress maintenance. The stress curve is therefore not subject to mass loss. The stress variation trends of the two forms of self-organization are almost the same, but both strengths are lower than that of unbroken particles. The crushing of the direct filling method specimens surges with increasing confining pressure. The effect of mass loss on stress variation starts to come to the fore. The volume loss effect due to the direct filling method is further enhanced at 500 kPa confining pressure. The difference between the two stress variation curves is more obvious, and even the difference between strain-softened and strain-hardened types appears. This is due to the reduction in the volume of the replacement sub-particles resulting in larger voids in the specimen. The stress concentration phenomenon tends to be obvious, and more

Figure 10 Stress–strain curves of two different crush.



(a) Volumetric strain curve



(b) Stress-strain curves

initial particles produce crushing. However, their volume loss leads to a larger single-particle ultimate strength, which has an inverse effect on the amount of crushing. At low confining pressure levels, this crushing equilibrium effect is not sufficient to affect

the stress trend. As the confining pressure level increases, it causes the crushing difference to be accentuated. From the simulation results, it can be concluded that there is a volume loss effect equilibrium point. Exceeding this point leads to a

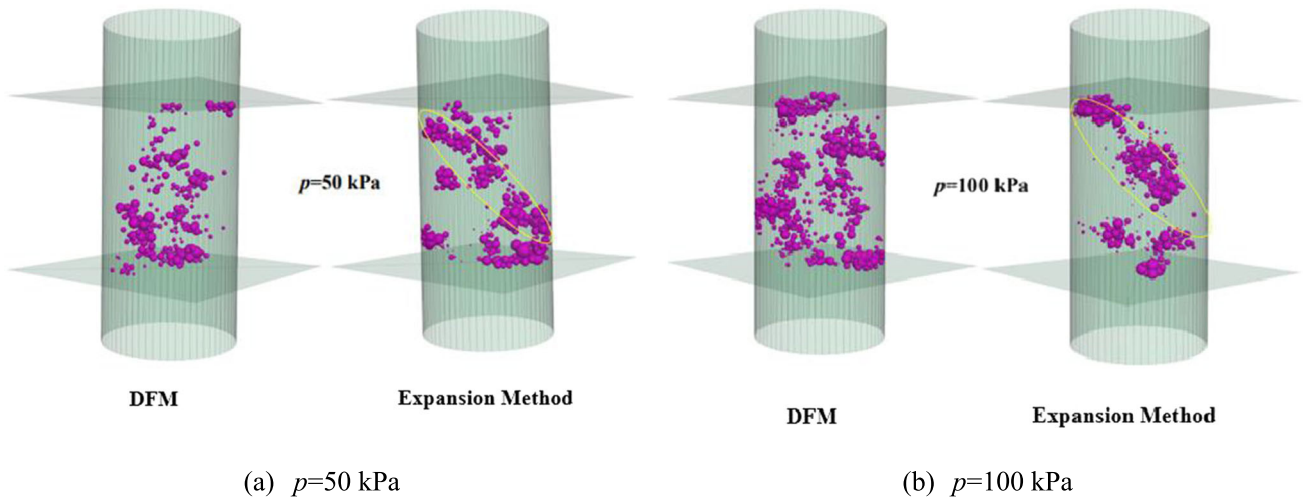


Figure 11 Comparison of broken bond of two samples under triaxial tests.

divergence of stress trends. Its positive promotion effect on the crushing volume starts to gradually exceed the negative hindrance effect. In contrast, the replacement sub-particles by expansion do not affect their ultimate strength and do not change the force conditions of the surrounding initial particles. This directly leads to the difference in the trend of stress change between the two. The particles in Fig. 11 are crushed particles. The crushed particles produced by the directly filling method are more dispersed, while the crushed particles produced by the expansion method are mostly concentrated within the circle. Meanwhile, it can be seen that the expansion method results in volume conserved specimen following a pattern of fragmentation along with the shear band.

The stress changes of the expansion method and the direct filling method converge again for the cases of 1 and 2 MPa of the confining pressure. This is since the fact that the ultimate strength of the latter sub-particles is higher than that of the former at high confining pressure levels. The reverse hindrance of crushing is enhanced by the direct filling method.

From the strain curves of the three specimens, it is clear that the volumetric strain of the unbroken specimens is only related to the degree of void compression. The dilatancy phenomenon eventually appeared in the specimens under each confining pressure condition. However, as the force level increases, the shear contraction is significantly enhanced while the shear dilatation is weakened. The shear contraction of the expansion method specimens is further enhanced compared to the uncrushed specimens. This is due to the filling of voids by small crushed particles, resulting in a further reduction of the volumetric strain. It is noteworthy that under the 500 kPa confining pressure condition, there is still a tendency for shear dilatation in the expanded specimens. The direct filling method is more fully crushed, resulting in increased porosity, smaller sub-particles, and more adequate filling of the voids. Affected by these two aspects, the shear contraction of the specimens is more obvious compared with the expansion method. With the increase of the confining pressure to more than 1 MPa, both crushed specimens were contracted, which also proved the existence of the equilibrium point of the volume loss effect.

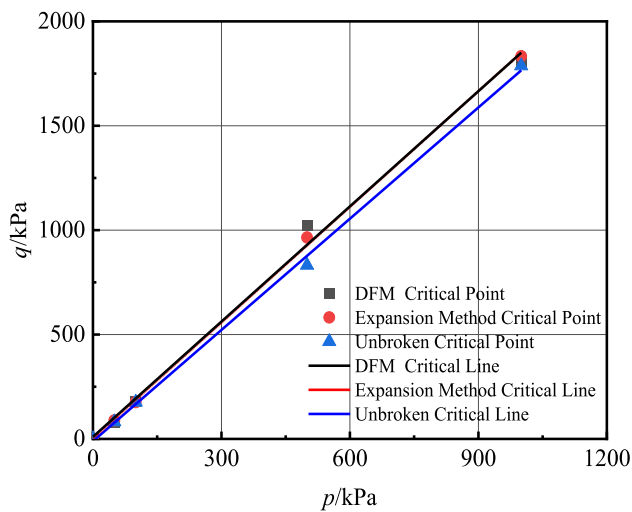
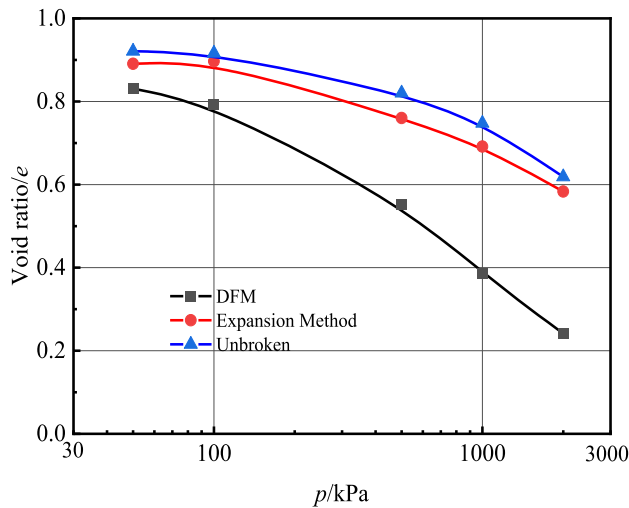
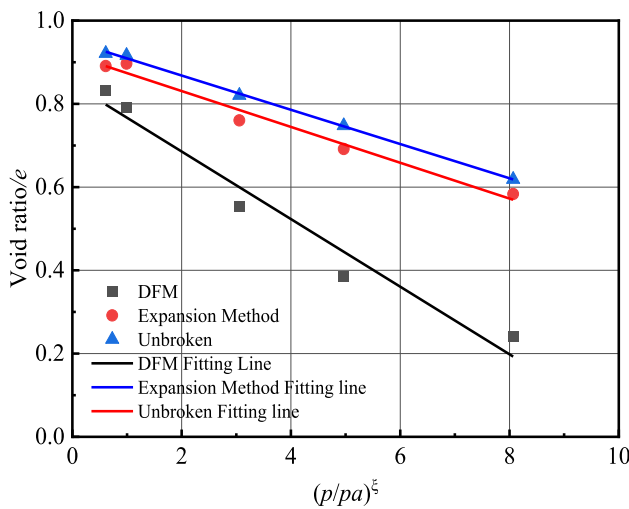


Figure 12 Critical state line in q - p plane.



(a) e - $\lg p$



(b) e - $(p/p_a)^{0.5}$

Figure 13 Critical state line in e - p plane.

Critical state lines

The critical state lines in the q - p plane are shown in Fig. 12 were obtained by critical state point fitting. The critical state lines of all three simulated specimens in this plane pass through the coordinate origin. All three fitting coefficients R^2 are up to 0.99 or more, which can be expressed by the equation $q = Mp$. The critical state stress ratio of unbroken particles is $M_{unbroken} = 1.762$, the critical state stress ratio of volume loss particles is $M_{loss} = 1.853$, and the critical state stress ratio of volume conserved particles is $M_{equal} = 1.851$. The critical state stress ratios of the two broken specimens are approximately equal.

Therefore, it can be seen that volume loss does not affect the final critical state stress ratio.

Figure 13a shows the distribution of the critical void ratio state points for the numerical tests of three different samples. Since the gradation and initial void ratio of the three are the same, the shift of the critical state line mainly comes from the difference in fragmentation. The state line where particle breakage does not occur is called the initial critical state line. From the fitting curve results of the critical state point, the initial critical state line gradually decreases with the increase of the confining pressure. The compression causes the critical void ratio to drop. The curve of the expansion method shifts overall to below the initial critical state line. The change of the critical void ratio is influenced by the initial void being compressed. At the same time, the filling of the specimen by crushed sub-particles leads to further compression. The specimens of the direct filling method did not affect the critical state line under the initial confining pressure. As the force level increases, the critical state line gradually shifts downward. The larger the confining pressure is, the larger the downward shift is. The volume loss has two effects on the critical state. On one hand, the particle volume reduction causes the porosity to be elevated and the compressibility to become stronger. The volumetric strain thus increases and there exists a positive effect on the compression. On the other hand, sub-particle volume loss and filling of voids by fine particles make the specimen denser and prevents the volume

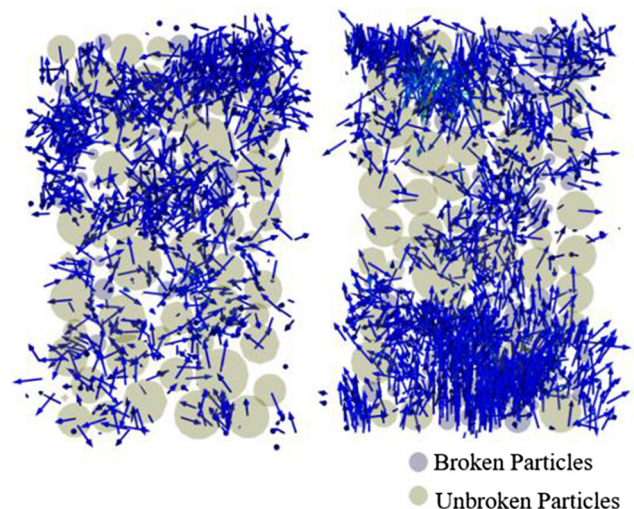


Figure 14 Particle trajectory of samples under 1 MPa confining pressure.

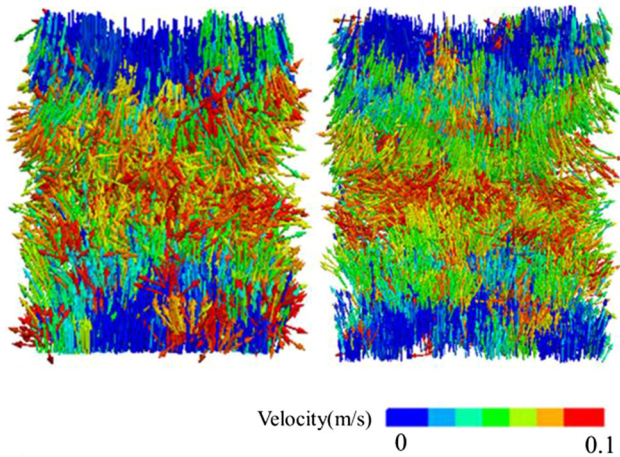


Figure 15 The particle velocity vector figure of samples under 1 MPa confining pressure.

from being compressed. The reduction in daughter particle volume leads to increased difficulty in crushing. This creates resistance to continued filling and produces a negative effect. However, the negative effect gradually decreases at large shear displacements. And the effect on the void ratio diminishes as the stress level increases.

Li et al. [43] found that the critical state lines in the $e - \lg p$ plane of sandy soils are irregular curves. However, it can be approximated by a straight line in the $e - (p/p_a)^\xi$ plane, which is given by

$$e_c = e_\Gamma - \lambda_c \left(\frac{p}{p_a} \right)^\xi \tag{11}$$

where e_c is the critical void ratio, e_Γ is the critical void ratio when the effective spherical stress is 0, λ_c is the slope of the critical line, ξ is the material parameter, which is taken as 0.7 in this paper, and P_a is the atmospheric pressure. The slopes of the fitted curves for the expansion method and the unbroken samples were 0.0431 and 0.0411, respectively, which were approximately parallel. While the slope of the direct filling method fitted straight line is 0.0812 and the fitting accuracy is lower than the other two lines as shown in Fig. 13b.

Microscale responses

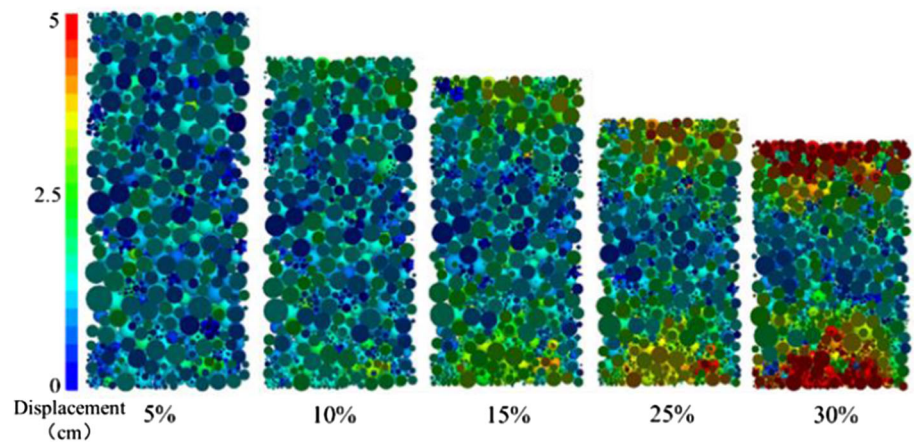
The trajectory of particle motion, as well as the particle motion velocity vector center profiles of the specimens under 1 MPa confining pressure, are given in Figs. 14 and 15. Both methods have intense motion in the particle crushing zone, while the motion at the

initial particles is not obvious. The trajectory of the direct filling method is mainly concentrated in the particle crushing region and shows disorder. While the overall motion trend of the expansion method is extended from the upper and lower loading plates to the middle of the specimen. The trajectory covers the broken particles, and the end triangle region is obviously broken. From the velocity vector, it can be seen that the sub-particles of the direct filling method are affected by the plunge at replacement and cannot maintain the original motion direction. The expansion method makes the upper and lower end tapered sections move approximately vertically, which can be identified as the elastic region. In the middle of the profile the velocity turns horizontally and the closer to the middle the more obvious the deflection is, showing a symmetrical decreasing phenomenon.

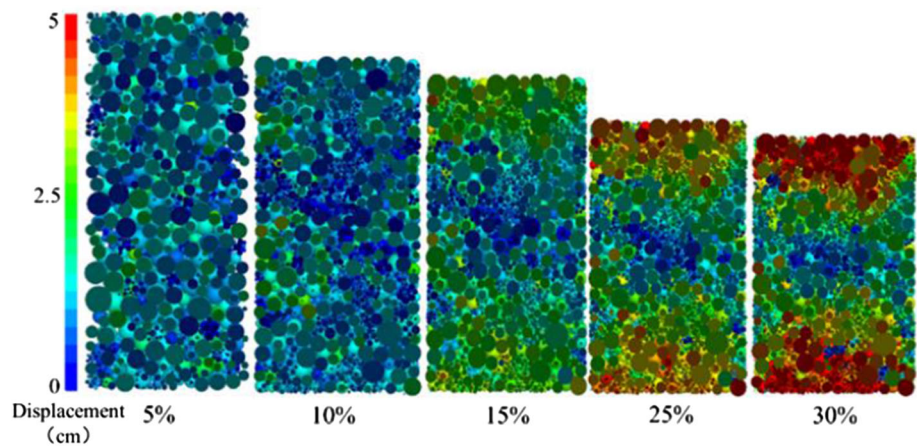
Figure 16 gives the displacement nephogram in the central longitudinal section under different strains of the two specimen numerical models. The comparison shows that the initial displacement development is approximately the same. As the axial strain increases, the difference in particle displacement is gradually accentuated. The direct filling method shows a certain regularity in shear morphology at the time of damage. That is, the end effect is obvious, but the particle displacement variability in the middle of the specimen is small and always shows uniform expansion. The overall displacement variation of the expansion method is more clear. Its nephogram better reflects the formation of the shear zone. The particles in the middle part of the specimen exhibit non-uniform dilatation when the specimen is damaged. This leads to a difference in displacement, which results in an “X” shaped distribution of the shear zone.

As the mechanism of force transmission in discrete elements, the evolution and distribution of the force chain play a crucial role. Figure 17 shows the central profile of force chain development under different axial strains. With the increase of axial strain, the force chain appears to develop gradually from an initial more uniform distribution toward the end. In combination with Figs. 15 and 16, the application of the expansion method results in a more regular movement of the end particles. The axial force chains are transferred early through the contact generated by the particle motion. The number of force chains is significantly more than that of the direct filling method specimens. With increasing shear

Figure 16 Numerical simulation displacement nephogram at different axial strains.



(a) DFM sample



(b) Expansion method sample

displacement, the force chain development tends to be consistent for the specimens of both methods. In addition, the coordination number, as an index to evaluate the overall contact stability of the specimens, is also important for the distribution of force chains. The critical coordination number of the volume conserved specimen is 5.212189, and the critical coordination number of the volume lost specimen is 5.154938. The difference between them is very small. The force chain distribution and the coordination number together determine that the critical stress ratios of the two methods are approximately equal.

Comparative analysis with physical tests

The effect of model parameters has a great influence on the simulation results, but the final simulation law obtained needs to be consistent with the triaxial experiment (Fig. 18). The triaxial test materials and

test conditions are shown in Table 5. Based on the consideration of the correctness of the numerical model, the influence of the expansion method on the simulation results is analyzed.

Figure 19 shows the comparison between the results of the expansion method and the physical experimental method under 400 kPa confining pressure, respectively. It can be seen that for the stress variation trend, the variability between the numerical simulation results and the experimental results is relatively small. However, the volume of the sub-particles plays a crucial role in the axial strain versus the volumetric strain. Both physical experiments and expansion method simulation results show significant shear dilatation. However, the direct filling method continuously maintains shear contraction with volume loss due to crushing. Although the stress changes of both the direct filling method and the expansion method meet the experimental results

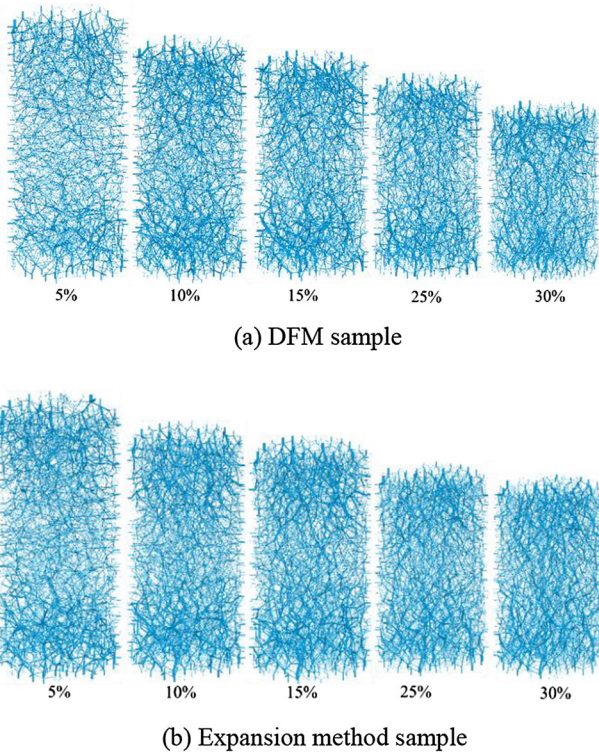


Figure 17 Development of contact force chain in the center section of samples under 1 MPa confining pressure.



Figure 18 Triaxial test specimen.

at lower envelope pressures, the difference in volumetric strains between the two is significant as the

Table 5 Test scheme

Sand type	Confining pressure(kPa)	Gs	Dry density(g/cm ³)	Drainage conditions
Calcareous sand	400	2.79	$\rho_{max} = 1.653$ $\rho_{min} = 1.267$	CD

crushing proceeds. Therefore, the expansion method ensured the reasonableness of the volume change.

Conclusions

A three-dimensional discrete element model is established based on the mass conservation and volume conservation considerations of daughter particle’s self-organization. The response of volume effect to macroscopic properties such as deformation characteristics, GSDs, and critical line variation is analyzed and concluded as follows.

1. The existence of the equilibrium point of the volume loss effect is verified. This point affects the stress–strain variability and is directly related to the stress level of the specimen. The softening curve is converted to hardening by the influence of this point. The volumetric strain is also influenced by this point from shear dilatation to shear contraction.
2. It can be seen that the difference in GSDs originates from the bidirectional influence of the volume loss of sub-particles on the crushing through quantitative analysis of the crushing rate and the number of particles. At a low-stress level, the volume loss promotes the crushing, and the gradation difference becomes larger with increasing stress levels. At a high-stress level, the volume loss hinders crushing and the gradation curve tends to move to the ultimate crushing curve and the difference becomes smaller.
3. The effect of volume loss on the critical state line is complex. Although the volume loss has a significant effect on the stress change during shear, it don’t affect the critical stress ratio. The decrease in the critical void ratio due to volume loss increases with the increase in the confining pressure.
4. From the microscopic displacement development, particle motion, and force chain development, it is clear that the microscopic

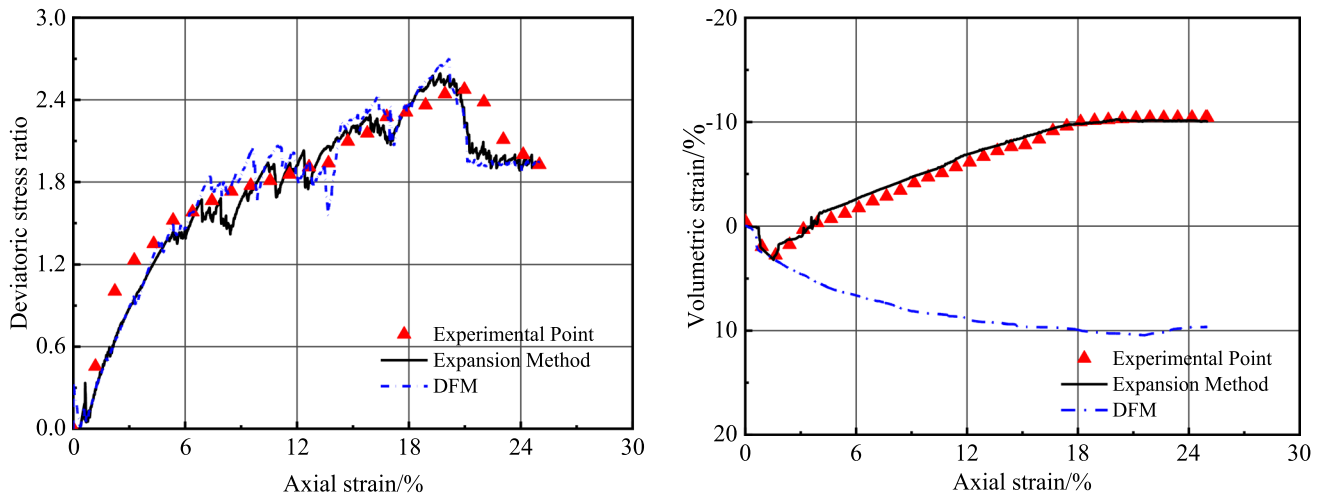


Figure 19 Results obtained by simulation methods and physical experiment.

characteristics of the expansion method are more consistent with the crushing law. Its macroscopic mechanical characteristics reflect more reasonably.

The expansion method is verified by the results of triaxial tests. The application of this method needs to be further research on experimental comparison studies. This study was only performed in same GSD. The macro and micro characteristics due to particle breakage needs to be investigated in other conditions.

Acknowledgements

This study was supported by the National Outstanding Youth Science Fund Project of the National Natural Science Foundation of China (Grant No. 51722801).

Data Availability

Some or all data, models, or code that support the findings of this study are available from the corresponding author upon reasonable request

Declarations

Conflict of interest No potential conflict of interest was reported by the authors.

References

- [1] Xiao Y, Liu H, Ding X, Chen Y, Jiang J, Zhang W (2016) Influence of particle breakage on critical state line of rockfill material. *Int J Geomech* 16(1):04015031. [https://doi.org/10.1061/\(ASCE\)GM.1943-5622.0000538](https://doi.org/10.1061/(ASCE)GM.1943-5622.0000538)
- [2] Koozhmishi M, Palassi M (2017) Effect of particle size distribution and subgrade condition on degradation of railway ballast under impact loads. *Granular Matter* 19(3):1–12. <https://doi.org/10.1007/s10035-017-0747-0>
- [3] Mark DS, Corinna R, Edmund PG (2001) *World Atlas of Coral Reefs*. University of California Press, Berkeley
- [4] Cundall PA, Strack O (2008) A discrete numerical model for granular assemblies. *Géotechnique* 30(3):331–336. <https://doi.org/10.1680/geot.1979.29.1.47>
- [5] Coop MR, Sorensen KK, Freitas TB, Georgoutsos G (2004) Particle breakage during shearing of a carbonate sand. *Géotechnique* 54(3):157–163. <https://doi.org/10.1680/geot.2004.54.3.157>
- [6] Ghafghazi M, Shuttle DA, Dejong JT (2014) Particle breakage and the critical state of sand. *Soils Found* 54(3):451–461. <https://doi.org/10.1016/j.sandf.2014.04.016>
- [7] Yu F (2017) Characteristics of particle breakage of sand in triaxial shear. *Powder Technol* 320:656–667. <https://doi.org/10.1016/j.powtec.2017.08.001>
- [8] Thornton C, Ciomocos MT, Adams MJ (1999) Numerical simulations of agglomerate impact breakage. *Powder Technol Lausanne* 105(1–3):74–82. [https://doi.org/10.1016/S0032-5910\(99\)00120-5](https://doi.org/10.1016/S0032-5910(99)00120-5)
- [9] Cheng YP, Nakata Y, Bolton MD (2003) Discrete element simulation of crushable soil. *Géotechnique* 53(7):633–641. <https://doi.org/10.1680/geot.2003.53.7.633>

- [10] Mcdowell GR, Harireche O (2002) Discrete element modelling of soil particle fracture. *Géotechnique* 52(2):131–135. <https://doi.org/10.1680/geot.2002.52.2.131>
- [11] Mcdowell GR, Harireche O (2002) Discrete element modelling of yielding and normal compression of sand. *Geotechnique* 52(4):299–304. <https://doi.org/10.1680/geot.2002.52.4.299>
- [12] Lobo-Guerrero S, Vallejo LE (2005) Crushing a weak granular material: experimental numerical analyses. *Géotechnique* 55(3):245–249. <https://doi.org/10.1680/geot.2005.55.3.245>
- [13] Marketos G, Bolton MD (2009) Compaction bands simulated in discrete element models. *J Struct Geol* 31(5):479–490. <https://doi.org/10.1016/j.jsg.2009.03.002>
- [14] Bono JP, Mcdowell GR (2014) DEM of triaxial tests on crushable sand. *Granular Matter* 16(4):551–562. <https://doi.org/10.1007/s10035-014-0500-x>
- [15] Bono JP, Mcdowell GR (2013) On the micro mechanics of one-dimensional normal compression. *Géotechnique* 63(11):895–908. <https://doi.org/10.1680/geot.12.P.041>
- [16] Åström MJ, Herrmann HJ (1998) Fragmentation of grains in a two-dimensional packing. *Physics of Condensed Matter* 570(83):551–554. <https://doi.org/10.1007/s100510050476>
- [17] Ciantia MO, Arroyo M, Calvetti F, Gens A (2015) An approach to enhance efficiency of DEM modelling of soils with crushable grains. *Géotechnique* 65(2):91–110. <https://doi.org/10.1680/geot.13.P.218>
- [18] Lobo-Guerrero S, Vallejo LE, Vesga LF (2006) Visualization of crushing evolution in granular materials under compression using DEM. *Int J Geomech* 6(3):195–200. [https://doi.org/10.1061/\(ASCE\)1532-3641\(2006\)6:3\(195\)](https://doi.org/10.1061/(ASCE)1532-3641(2006)6:3(195))
- [19] Ben-Nun O, Einav I (2010) The role of self-organization during confined comminution of granular materials. *Philos Trans A Math Phys Eng* 368(1910):231–247. <https://doi.org/10.1098/rsta.2009.0205>
- [20] Shi DD, Cao D, Deng Y, Xue J (2020) Dem investigations of the effects of intermediate principal stress ratio and particle breakage on the critical state behaviors of granular soils. *Powder Technol* 379(3):547–559. <https://doi.org/10.1016/j.powtec.2020.10.094>
- [21] Cleary PW (2001) Recent advances in DEM modelling of tumbling mills. *Miner Eng* 14(10):1295–1319. [https://doi.org/10.1016/S0892-6875\(01\)00145-5](https://doi.org/10.1016/S0892-6875(01)00145-5)
- [22] Cleary PW, Sinnott MD (2015) Simulation of particle flows and breakage in crushers using DEM: Part 1-Compression crushers. *Miner Eng* 74:178–197. <https://doi.org/10.1016/j.mineng.2014.10.021>
- [23] Li HQ, McDowell G, Lowndes I (2014) Discrete element modelling of a rock cone crusher. *Powder Technol* 263:151–158. <https://doi.org/10.1016/j.powtec.2014.05.004>
- [24] Yue P, De Bono JP, Yu HS, Mcdowell GR (2013) Micro mechanics of isotropic normal compression. *Géotechnique Letters* 3(4):166–172. <https://doi.org/10.1680/geolett.13.00050>
- [25] Bono JP, Mcdowell GR (2018) Micro mechanics of drained and undrained shearing of compacted and overconsolidated crushable sand. *Géotechnique* 68(7):575–589. <https://doi.org/10.1680/jgeot.16.P.318>
- [26] Zhou W, Yang L, Ma G, Chang X, Cheng Y, Li D (2015) Macro–micro responses of crushable granular materials in simulated true triaxial tests. *Granular Matter* 17(4):497–509. <https://doi.org/10.1007/s10035-015-0571-3>
- [27] Ben-Nun O, Einav I, Tordesillas A (2010) Force attractor in confined comminution of granular materials. *Phys Rev Lett* 104(10):108001. <https://doi.org/10.1103/PhysRevLett.104.108001>
- [28] Carslaw HS, Jaeger JC (1940) Some Two-Dimensional Problems in Conduction of Heat with Circular Symmetry. *Proc Lond Math Soc* 46(1):361–388. <https://doi.org/10.1112/plms/s2-46.1.361>
- [29] De Bono J, Mcdowell GR (2016) Particle breakage criteria in discrete-element modelling. *Géotechnique* 66(12):1014–1027. <https://doi.org/10.1680/jgeot.15.P.280>
- [30] Russell AR, Wood DM (2009) Point load tests and strength measurements for brittle spheres. *Int J Rock Mech Min Sci* 46(2):272–280. <https://doi.org/10.1016/j.ijrmms.2008.04.004>
- [31] Russell AR, Wood DM, Kikumoto M (2009) Crushing of particles in idealised granular assemblies. *J Mech Phys Solids* 57(8):1293–1313. <https://doi.org/10.1016/j.jmps.2009.04.009>
- [32] Hiramatsu Y, Oka Y (1966) Determination of the tensile strength of rock by a compression test of an irregular test piece. *Int J Rock Mech Min Sci Geomech Abstr* 3(2):89–90. [https://doi.org/10.1016/0148-9062\(66\)90002-7](https://doi.org/10.1016/0148-9062(66)90002-7)
- [33] Christensen RM (2000) Yield functions, damage states, and intrinsic strength. *Math Mech Solids* 5(3):285–300. <https://doi.org/10.1177/108128650000500302>
- [34] Weibull W (1951) A statistical distribution function of wide applicability. *Jour App Mech* 18:293–297. <https://doi.org/10.1115/1.4010337>
- [35] Mcdowell GR (2002) On the yielding and plastic compression of sand. *Soils Found* 42(1):139–145. <https://doi.org/10.3208/sandf.42.1139>
- [36] Borkovec M, Paris WD, Peikert R (1994) The fractal dimension of the apollonian sphere packing. *Fractals-complex Geom Patterns Scaling Nat Soc* 2(04):521–526. <https://doi.org/10.1142/S0218348X94000739>
- [37] Ciantia MO, Arroyo M, O’Sullivan C, Gens A, Liu T (2018) Grading evolution and critical state in a discrete numerical

- model of Fontainebleau sand. *Géotechnique* 69(1):1–15. <https://doi.org/10.1680/jgeot.17.P.023>
- [38] Roscoe K, Schofield AN, Wroth CP (1958) On Yielding Soils *Géotechnique* 8(1):22–53. <https://doi.org/10.1680/geot.1958.8.1.22>
- [39] Marsal RJ (1967) Large-scale testing of rockfill materials. *J Soil Mech Found Division* 93(2):27–43. <https://doi.org/10.1061/JSFEAQ.0000958>
- [40] Lade PV, Yamamuro JA, Bopp PA (1996) Significance of particle crushing in granular materials. *J Geotechn Eng* 122(4):309–316. [https://doi.org/10.1061/\(ASCE\)0733-9410\(1996\)122:4\(309\)](https://doi.org/10.1061/(ASCE)0733-9410(1996)122:4(309))
- [41] Hardin BO (1985) Crushing of soil particles. *J Geotechn Eng* 111(10):1177–1192. [https://doi.org/10.1061/\(ASCE\)0733-9410\(1985\)111:10\(1177\)](https://doi.org/10.1061/(ASCE)0733-9410(1985)111:10(1177))
- [42] Einav I (2007) Breakage mechanics part I: theory. *J Mech Phys Solids* 55(6):1274–1297. <https://doi.org/10.1016/j.jmps.2006.11.003>
- [43] Li XS, Dafalias YF (2000) Dilatancy for cohesionless soils *Géotechnique* 50(4):449–460. <https://doi.org/10.1680/geot.2000.50.4.449>

Publisher's Note Springer Nature remains neutral with regard to jurisdictional claims in published maps and institutional affiliations.

Springer Nature or its licensor (e.g. a society or other partner) holds exclusive rights to this article under a publishing agreement with the author(s) or other rightsholder(s); author self-archiving of the accepted manuscript version of this article is solely governed by the terms of such publishing agreement and applicable law.